Reprinted from Journal of the Optical Society of America A, Vol. 3, page 319, March 1986

Tiny core or thin layer as a perturbation in scattering by a single-layered sphere

Ramesh Bhandari

Applied Laser/Optics Group, Department of Physics, New Mexico State University, Las Cruces, New Mexico 88003

Received February 11, 1985; accepted October 23, 1985

Analytic expressions for scattering by a single-layered sphere when either the core is tiny or the shell thickness is small are presented within the framework of a perturbative approach. In this approach, the contribution of the core or the shell (each acting as a perturbation) to the scattering is separated out, thus facilitating a deeper insight into the nature of its effect. This is illustrated by the application of the analytic expressions to the well-known practical case of absorption of visible light by water droplets contaminated with graphitic carbon (soot) in the atmosphere.

1. INTRODUCTION

In this paper, we consider a perturbative approach to scattering by a single-layered sphere (Fig. 1) when either the core is tiny or the layer is thin. The approximation procedure leads in each case to the formulation of the scattering amplitude as the sum of the Mie scattering amplitude corresponding to the voluminous material and the perturbative correction term resulting from the presence of the other material in a relatively scant amount. Clearly, this manner of expressing the scattering amplitudes for the single-layered sphere permits one to study the effect of the perturbing material separately in detail.

We begin by stating the exact analytic expressions for scattering by a single-layered case in Section 2 and subsequently deal in detail with the case of a tiny core embedded at the center of a sphere in Section 3, followed by the case of a thin shell around a spherical particle in Section 4. Section 5 is the conclusion. Appendix A gives the boundary conditions at a thin spherical layer.

The results of our approximation scheme are applied to the case of absorption of visible light by water droplets contaminated with graphitic carbon (soot) in the atmosphere. This case is of practical interest with important implications for climatology and has attracted a great deal of attention in the past. In 1965, Fenn and Oser[1] considered the scattering of a water droplet with a soot core. Subsequently, in 1969, Danielson *et al.*[2] applied this model in their study of the transfer of visible radiation through clouds. Increasing evidence of the presence of soot in the atmosphere has renewed further interest in the impact of soot on climate.[3,4] Recently, Chylek *et al.*[5] investigated in detail the effect of soot on the albedo of clouds by using different models of soot–water mixture. Our application of the results to the soot–water mixture, when soot exists as a tiny core or a thin shell, reveals some novel features of the absorption process within the framework of such models. Numerical results in the case of the thin-shell case indicate in a general way that the absorption cross section per unit volume of an absorbing material, under appropriate conditions, could be enhanced by several orders of magnitude. This result is interesting because of the importance of the value of this parameter in the studies of the effect of mixing of an absorbing material with a nonabsorbing or a weakly absorbing material.[5]

2. SINGLE-LAYERED SPHERE

In general, the partial-wave scattering amplitudes for a plane wave incident upon a single-layered sphere can be written as[6,7]

$$a_n = \frac{N_n}{D_n}, \tag{1}$$

$$b_n = \frac{M_n}{C_n}, \tag{2}$$

where

$$N_n = \begin{vmatrix} \psi_n(x_2) & m_2\psi_n(m_2x_2) & m_2\chi_n(m_2x_2) & 0 \\ \psi'_n(x_2) & \psi'_n(m_2x_2) & \chi'_n(m_2x_2) & 0 \\ 0 & m_2\psi_n(m_2x_1) & m_2\chi_n(m_2x_1) & m_1\psi_n(m_1x_1) \\ 0 & \psi'_n(m_2x_1) & \chi'_n(m_2x_1) & \psi'_n(m_1x_1) \end{vmatrix}, \tag{3}$$

$$D_n = \begin{vmatrix} \zeta_n(x_2) & m_2\psi_n(m_2x_2) & m_2\chi_n(m_2x_2) & 0 \\ \zeta'_n(x_2) & \psi'_n(m_2x_2) & \chi'_n(m_2x_2) & 0 \\ 0 & m_2\psi_n(m_2x_1) & m_2\chi_n(m_2x_1) & m_1\psi_n(m_1x_1) \\ 0 & \psi'_n(m_2x_1) & \chi'_n(m_2x_1) & \psi'_n(m_1x_1) \end{vmatrix}, \tag{4}$$

$$M_n = \begin{vmatrix} \psi_n(x_2) & \psi_n(m_2x_2) & \chi_n(m_2x_2) & 0 \\ \psi'_n(x_2) & m_2\psi'_n(m_2x_2) & m_2\chi'_n(m_2x_2) & 0 \\ 0 & \psi_n(m_2x_1) & \chi_n(m_2x_1) & \psi_n(m_1x_1) \\ 0 & m_2\psi'_n(m_2x_1) & m_2\chi'_n(m_2x_1) & m_1\psi'_n(m_1x_1) \end{vmatrix}, \tag{5}$$

0740-3232/86/030319-10$02.00

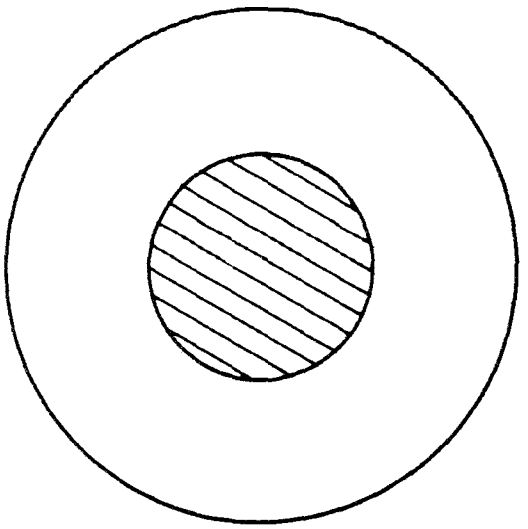

Fig. 1. A single-layered sphere.

$$C_n = \begin{vmatrix} \zeta_n(x_2) & \psi_n(m_2x_2) & \chi_n(m_2x_2) & 0 \\ \zeta'_n(x_2) & m_2\psi'_n(m_2x_2) & m_2\chi'_n(m_2x_2) & 0 \\ 0 & \psi_n(m_2x_1) & \chi_n(m_2x_1) & \psi_n(m_1x_1) \\ 0 & m_2\psi'_n(m_2x_1) & m_2\chi'_n(m_2x_1) & m_1\psi'_n(m_1x_1) \end{vmatrix}, \quad (6)$$

$$x_i = 2\pi r_i/\lambda, \quad (7)$$

where λ is the wavelength of the incident wave and r_1 and r_2 are the inner and the outer radii of the shell, respectively. m_1 and m_2 denote the refractive indices of the material in the core and within the shell, respectively. The Ricatti–Bessel functions are

$$\psi_n(z) = zj_n(z),$$
$$\chi_n(z) = -zn_n(z),$$
$$\zeta_n(z) = zh_n^{(2)}(z), \quad (8)$$

where j_n, n_n, and $h_n^{(2)}$ are the spherical Bessel, Neumann, and Hankel functions of the second kind, respectively.

The extinction cross section, the scattering cross section, and the absorption cross section are calculated from a_n and b_n in the following way:

$$\sigma_{\text{ext}} = \frac{\lambda^2}{2\pi}\sum_{n=1}^{\infty}(2n+1)\text{Re}(a_n + b_n),$$

$$\sigma_{\text{sca}} = \frac{\lambda^2}{2\pi}\sum_{n=1}^{\infty}(2n+1)(|a_n|^2 + |b_n|^2),$$

$$\sigma_{\text{abs}} = \sigma_{\text{ext}} - \sigma_{\text{sca}} = \frac{\lambda^2}{2\pi}\sum_{n=1}^{\infty}(2n+1) \times [\text{Re}(a_n + b_n) - (|a_n|^2 + |b_n|^2)]. \quad (9)$$

3. TINY CORE

The scattering amplitude of a_n of Eq. (1) can be recast in the form

$$a_n = a_n^{(h)}\left[\frac{1 - (\beta_n/\alpha_n)\hat{N}_n^{(h)}/N_n^{(h)}}{1 - (\beta_n/\alpha_n)\hat{D}_n^{(h)}/D_n^{(h)}}\right], \quad (10)$$

where

$$a_n^{(h)} = N_n^{(h)}/D_n^{(h)} \quad (11)$$

is the Mie scattering amplitude corresponding to a homogeneous sphere characterized by parameters m_2 and x_2 and

$$N_n^{(h)} = \psi_n(x_2)\psi'_n(m_2x_2) - m_2\psi'_n(x_2)\psi_n(m_2x_2),$$
$$D_n^{(h)} = \zeta_n(x_2)\psi'_n(m_2x_2) - m_2\zeta'_n(x_2)\psi_n(m_2x_2),$$
$$\hat{N}_n^{(h)} = \psi_n(x_2)\chi'_n(m_2x_2) - m_2\psi'_n(x_2)\chi_n(m_2x_2),$$
$$\hat{D}_n^{(h)} = \zeta_n(x_2)\chi'_n(m_2x_2) - m_2\zeta'_n(x_2)\chi_n(m_2x_2),$$
$$\alpha_n = m_2\psi'_n(m_1x_1)\chi_n(m_2x_1) - m_1\psi_n(m_1x_1)\chi'_n(m_2x_1),$$
$$\beta_n = m_2\psi'_n(m_1x_1)\psi_n(m_2x_1) - m_1\psi_n(m_1x_1)\psi'_n(m_2x_1). \quad (12)$$

Except for α_n and β_n, all the expressions above involve x_2. We now assume that $|m_1|x_1 \ll 1$ and $|m_2|x_1 \ll 1$. Consequently, in α_n and β_n we use the fact that, in the limit $z \to 0$,

$$\psi_n(z) = z^{n+1}/G_{1n},$$
$$\psi'_n(z) = (n+1)z^n/G_{1n},$$
$$\chi_n(z) = G_{2n}/z^n,$$
$$\chi'_n(z) = -nG_{2n}/z^{n+1}, \quad (13)$$

where

$$G_{1n} = 1 \times 3 \times 5 \ldots (2n+1),$$
$$G_{2n} = 1 \times 3 \times 5 \ldots (2n-1). \quad (14)$$

Retaining the most leading terms,

$$\beta_n/\alpha_n = \frac{-(2n+1)(n+1)(m_2x_1)^{2n+1}(m_1^2 - m_2^2)}{(G_{1n})^2[nm_1^2 + m_2^2(n+1)]}. \quad (15)$$

Equation (10) can now be written as

$$a_n = a_n^{(h)}\{1 - (\beta_n/\alpha_n)[\hat{N}_n^{(h)}/N_n^{(h)} - \hat{D}_n^{(h)}/D_n^{(h)}]\}. \quad (16)$$

One can further show that the bracketed expression multiplying (β_n/α_n) reduces to $-im_2/[N_n^{(h)}D_n^{(h)}]$. As a result,

$$a_n = a_n^{(h)} + f_n, \quad (17)$$

where the correction term f_n is

$$f_n = m_2(-i\beta_n/\alpha_n)(-1)/[D_n^{(h)}]^2, \quad (18)$$

with (β_n/α_n) given by Eq. (15). The quantity $(-i\beta_n/\alpha_n)$ corresponds to the scattering amplitude for a plane wave traveling in a continuous homogeneous medium with refractive index m_2 and incident upon a tiny homogeneous sphere (parameters m_1 and x_1) embedded in such a medium. If one further recognizes that $i/D_n^{(h)}$ = the coefficient associated with the field inside a homogeneous sphere (parameters m_2 and x_2), the factor $-[1/D_n^{(h)}]^2$ in the expression for f_n may be interpreted as

a necessary modification to $-i(\beta_n/\alpha_n)$, since the wave incident upon the core (radius r_1) is not the initial plane wave but the field inside the larger sphere (radius r_2). Moreover, the wave scattered by the core is being detected not within the medium of refractive index m_2 but outside the larger sphere where the refractive index is 1. This also explains the extra factor of m_2 in Eq. (18) (see the Fresnel coefficient for transmission of light[6]).

In a similar fashion, one shows that the partial-wave scattering amplitudes b_n in the presence of a tiny core can be expressed as

$$b_n = b_n^{(h)} + g_n, \tag{19}$$

where $b_n^{(h)}$ is the Mie partial-wave scattering amplitude for a homogeneous sphere characterized by parameters m_2 and x_2 and g_n is the lowest-order correction term given by

$$g_n = im_2(\gamma_n/\delta_n)/[C_n^{(h)}]^2, \tag{20}$$

where

$$\gamma_n/\delta_n = \frac{-(m_2x_1)^{2n+3}(m_1^2/m_2^2 - 1)}{G_{1n}^2(2n+3)}. \tag{21}$$

$C_n^{(h)}$ is the denominator that occurs in the expression of the scattering amplitude

$$b_n^{(h)} = M_n^{(h)}/C_n^{(h)} \tag{22}$$

and is given by

$$C_n^{(h)} = m_2\zeta_n(x_2)\psi'_n(m_2x_2) - \zeta'_n(x_2)\psi_n(m_2x_2). \tag{23}$$

The factors (γ_n/δ_n) and $i/C_n^{(h)}$ have similar interpretations, as in the case of the correction to $a_n^{(h)}$ amplitude.

In the calculation of cross sections given in Eqs. (9), the most leading effect of the core arises from the correction term corresponding to the amplitude $a_1^{(h)}$. This correction term f_1 [see Eq. (18)] is the Rayleigh-scattering term $-i\beta_1/\alpha_1$ [see Eq. (15)] modified as explained before. Setting

$$f_n = \delta_{n1}f_1, \qquad n = 1, 2, \ldots \tag{24a}$$

and

$$g_n = 0, \qquad n = 1, 2, \ldots, \tag{24b}$$

the various cross sections with the lowest-order correction are

$$\sigma_{ext} = \sigma_{ext}^{(h)} + \frac{3\lambda^2}{2\pi}\,\mathrm{Re}(f_1), \tag{25a}$$

$$\sigma_{sca} = \sigma_{sca}^{(h)} + \frac{3\lambda^2}{2\pi}\,2\,\mathrm{Re}\{[a_1^{(h)}]^* f_1\}, \tag{25b}$$

$$\sigma_{abs} = \sigma_{abs}^{(h)} + \frac{3\lambda^2}{2\pi}\,\mathrm{Re}\,(f_1\{1 - 2[a_1^{(h)}]^*\}). \tag{25c}$$

The superscript h refers to scattering by a homogeneous sphere characterized by parameters m_2, x_2. If this sphere is nonabsorbing $[\sigma_{abs}^{(h)} = 0]$, Eq. (25c), with f_1 given by Eqs. (18) and (15), reduces to

$$\sigma_{abs} = \frac{(3\lambda^2)}{2\pi}\,m_2\,\mathrm{Im}\left[\frac{-(2/3)(m_2x_1)^3(m_1^2 - m_2^2)}{m_1^2 + 2m_2^2}\right]\frac{1}{|D_1^{(h)}|^2}, \tag{26}$$

which corresponds to absorption in the Rayleigh region modified by factors, as discussed earlier.

One of the quantities of interest in the study of the effect of mixing of absorbing material with a nonabsorbing material is the absorption cross section per unit volume (or mass) of the absorbing material.[8] Denoting the volume of the absorbing material by V and using Eq. (26), one obtains

$$\sigma_{abs}/V = \frac{-6\pi m_2^4}{\lambda}\,\mathrm{Im}\left[\frac{(m_1^2 - m_2^2)}{m_1^2 + 2m_2^2}\right]\Big/|D_1^{(h)}|^2, \tag{27}$$

which is independent of the size of the core, a familiar result in Rayleigh scattering. As an illustration, we consider the absorption of visible light by a tiny graphitic-carbon (soot) core at the center of a water droplet. This is a case of practical interest in the study of scattering of light by fog or clouds. For calculations, we choose $r_2 = 5\ \mu$m, $\lambda = 0.5\ \mu$m, m_2 (water) = $1.33 - i0.00$, and $m_1 = 2.0 - im_I$. For the special case of soot, we take $m_I = 0.66$. Figure 2 shows the plot of σ_{abs}/V as a function of the volume fraction F of absorbing material for different values of m_I. The top curve corresponds to absorption by graphitic carbon (soot). Each curve was obtained by using the exact analytic expressions for a single-layered sphere given in Section 2. The numerical procedure employed is the procedure suggested in Ref. 7. We see in Fig. 2 that the common characteristic of the curves is a flatness in the value of σ_{abs}/V that sets in below $F = 10^{-7}$. This regime corresponds to Rayleigh scattering, as can be seen by evaluating m_2x_1. For $F = 10^{-7}$, $m_2x_1 = 0.4$. The limiting value in each curve is precisely the value that one obtains from Eq. (27). This agreement, we may mention, is also a test of the numerical stability of our computational procedure outlined in Ref. 7. We also note that significant deviation from flatness occurs essentially when F exceeds 10^{-6}.

We also remark here that, for small values of m_I, Eq. (27) predicts the limiting value to be proportional to m_I, which is verified in Fig. 2. The fact that σ_{abs}/V is independent of m_I above $F = 10^{-4}$ can be explained by the fact that, for such

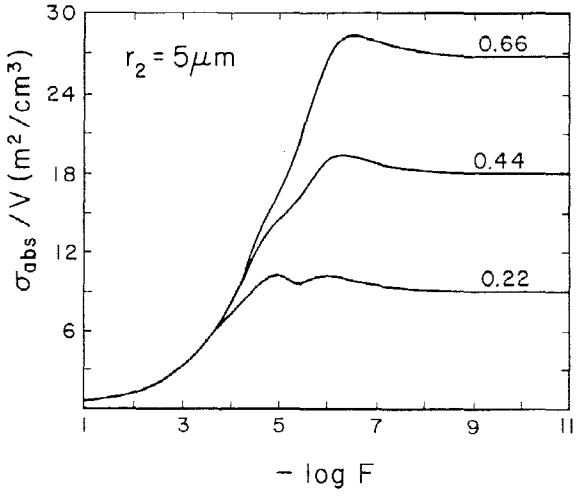

Fig. 2. Absorption cross section of water droplet ($m_2 = 1.33 - i0.0$) per unit volume of the core ($m_1 = 2.0 - im_I$, $m_I > 0$) denoted by $\sigma_{abs/V}$ as a function of its volume fraction F. The radius of the water droplet $r_2 = 5\ \mu$m and the wavelength of light $\lambda = 0.5\ \mu$m. Each curve is labeled by the value of m_I. $m_I = 0.66$ corresponds to graphitic carbon (soot).

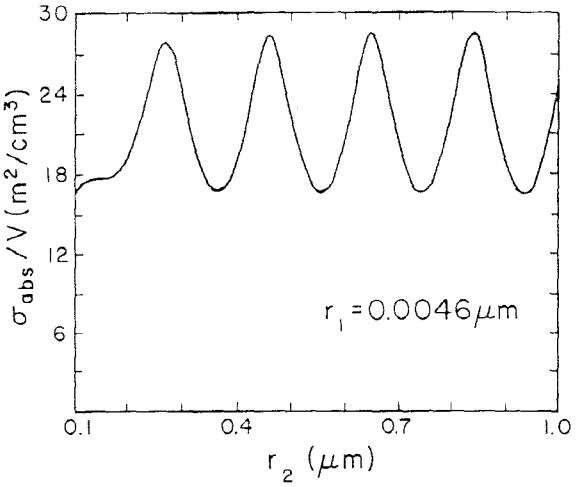

Fig. 3. σ_{abs}/V as a function of the radius r_2 of the water droplet. The soot core ($m_1 = 2.0 - i0.66$) has a fixed radius $r_1 = 0.0046\ \mu m$.

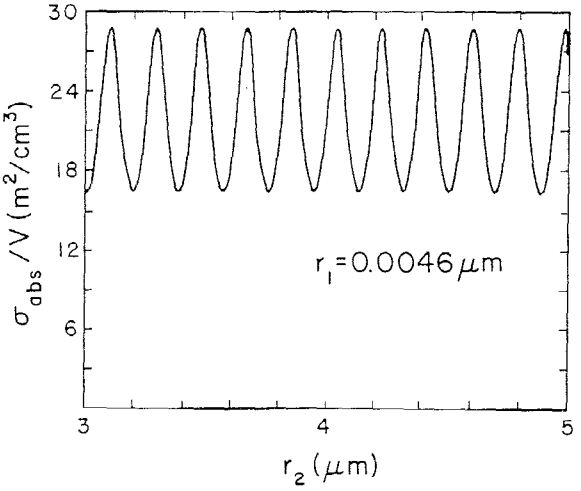

Fig. 4. Same as Fig. 3, but for larger water droplets.

volume fractions, the radius of the core is large enough to absorb essentially all the light incident upon it, regardless of the imaginary part of the refractive index considered in Fig. 2. To understand this, we compare the skin depth given by $\delta = (\lambda/m_2)/(2\pi m_I)$ with the radius of the core (absorbing material). For the values of m_I considered in Fig. 2, the largest value of δ (which corresponds to $m_I = 0.22$). is 0.27 μm, whereas the value of the core radius r_1 corresponding to $F = 10^{-4}$ is 0.23 μm. The rough equality of these two quantities shows why the curves of Fig. 2 merge below $F = 10^{-4}$.

Equation (27) also shows that the dependence of σ_{abs}/V on the outer radius r_2 is expressed through the factor $1/|D_1^{(h)}|^2$, where $D_1^{(h)}$ is given by

$$D_1^{(h)} = \zeta_1(x_2)\psi'_1(m_2x_2) - m_2\zeta'_1(x_2)\psi_1(m_2x_2). \quad (28)$$

In the limit $x_2 \gg 1$, this expression reduces to

$$D_1^{(h)} = \exp(-ix_2)[\sin(m_2x_2) - im_2\cos(m_2x_2)]. \quad (29)$$

Furthermore, when m_2 is real,

$$1/|D_1^{(h)}|^2 = 1/[1 + (m_2^2 - 1)\cos^2(m_2x_2)], \quad (30)$$

which implies that extrema occur in the value of σ_{abs}/V whenever $m_2x_2 = (2n + 1)\pi/2$ or $m_2x_2 = n\pi$, where n is an integer. Figure 3 shows the plot of σ_{abs}/V as a function of r_2 for $r_1 = 0.0046\ \mu m$, $m_I = 0.66$, with the rest of the parameters being the same as the earlier ones. Calculations were again carried out based on the exact expressions of Section 2 and the calculational procedure of Ref. 7. $m_2x_1 = 0.077$, implying that the core is always in the Rayleigh region. Consequently, Eq. (27) remains valid. In Fig. 3, we see the oscillations predicted by Eq. (30). The first prominent peak corresponds roughly to $m_2x_2 = 3\pi/2$, consistent with the fact that x_2 is much greater than 1. Subsequent peaks are given by $m_2x_2 = (2n + 1)\pi/2$, $n = 2, 3, 4$. This oscillating pattern continues beyond $r_2 = 1\ \mu m$. In Fig. 4, we have shown this pattern for r_2 between 3 and 5 μm. At $r_2 = 5\ \mu m$, we get the same value as in Fig. 2. The distance between any two consecutive peaks is given by $\Delta r_2 = \lambda/(2m_2) = 0.19\ \mu m$, and the ratio of the maximum to the minimum is $m_2^2 = 1.77$. These results are verified in Figs. 3 and 4. It may be mentioned that such oscillations dominated by the Rayleigh term are observed even beyond the value of 0.05 μm for the core radius. For example, for $r_1 = 0.05\ \mu m$, the mean value in the region of oscillations is around 25 m^2/cm^3, which is slightly larger than the mean value corresponding to Fig 4. These values are to be compared with a maximum value of 13 m^2/cm^3 in a polydispersion of carbon particles in air. The maximum value corresponds to a carbon-particle radius of about 0.08 μm.

It is important to remark here that the prominent peaks of Figs. 3 and 4 may be regarded as resonances in the internal field of the water droplet. This is so since each peak is associated with a complex pole. That is, the denominator $D_1^{(h)}$ of Eq. (29) has a complex zero in the vicinity of each peak. The real part of this zero is the same as the position of the peak, which is given by $m_2x_2 = (2n + 1)\pi/2$ ($x_2 \gg 1$). On the other hand, the imaginary part of each zero has a common value p given by

$$p = [1/(2m_2)]\ln[(m_2 + 1)/(m_2 - 1)]. \quad (31)$$

If $m_2 \gg 1$, we see at once that $p = 1/m_2^2$, with the poles very close to the real x_2 axis. The peaks correspondingly become

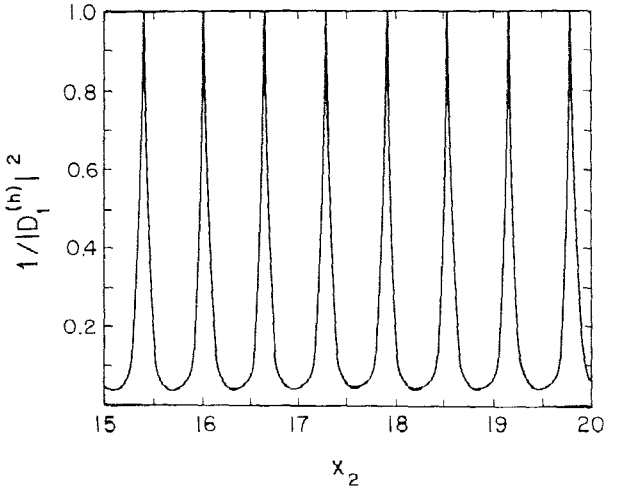

Fig. 5. A plot of $1/|D_1^{(h)}|^2$ versus the size parameter $x_2 = 2\pi r_2/\lambda$ depicting the sharp resonant behavior when the refractive index $m_2 = 5.0$. $1/|D_1^{(h)}|^2$ is the modulus square of the internal field coefficient associated with the scattering amplitude $a_1^{(h)}$ for a homogenous spherical particle.

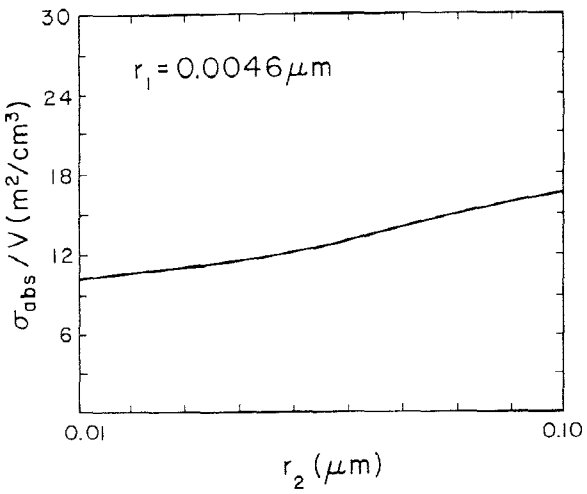

Fig. 6. The lower end of the curve indicates the approach to the Rayleigh-scattering limit for the composite particle (soot core + water shell) in air.

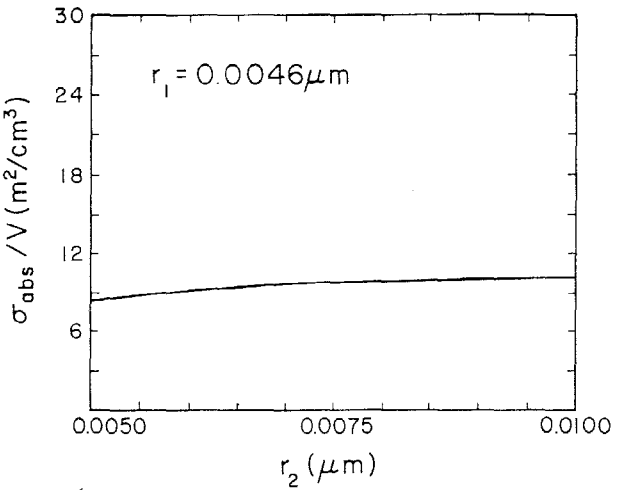

Fig. 7. The lower end of this curve corresponds essentially to Rayleigh absorption by the carbon particle (radius $r_1 = 0.0046\ \mu m$) in air.

very narrow [see also Eq. (30)] dropping sharply from their maximum value of 1 to the minimum value of $1/m_2^2$, which approaches zero rapidly as m_2 becomes large. This is shown in Fig. 5. However, for the case under consideration, $m_2 = 1.33$ and p [given by Eq. (31)] is 0.73. Consequently, the resonance effect here is weaker compared with the case illustrated in Fig. 5. One also sees from Eqs. (27) and (30) that the maximum value of σ_{abs}/V, which corresponds to the peaks of Fig. 4, increases with m_2, the refractive index of the surrounding (nonabsorbing) shell. For $m_2 \gg |m_1|$, this maximum value is proportional to m_2^2.

In Fig. 6, the flatness approached by the curve near the lower end of the curve is due to the onset of Rayleigh scattering for the composite particle and is described by the expression

$$\sigma_{abs}/V = \frac{-54\pi m_2^2}{\lambda(2+m_2^2)^2}\,\mathrm{Im}\left\{\frac{m_1^2 - m_2^2}{m_1^2 + 2m_2^2}\right\}, \tag{32}$$

which is obtained from Eq. (27) after making the appropriate approximation for $D_1^{(h)}$. For the parameters considered for the curve in Fig. 4, the value from Eq. (32) is 10.3 m^2/cm^3, which is in agreement with the limiting value indicated by the curve in Fig. 6. However, if r_2 is decreased further to a value close to r_1 (see Fig. 7), σ_{abs}/V approaches the value corresponding to Rayleigh absorption by carbon particles in air or in vacuum ($m_2 = 1$). This limit is given by Eq. (32) with $m_2 = 1$. The value is 8.4 m^2/cm^3 and agrees with the curve of Fig. 7.

4. THIN SHELL

In this section, we explore the consequences of a thin shell around a spherical particle.

When the shell thickness is small, all the Ricatti–Bessel functions and their derivatives involving the size parameter x_1 in Eqs. (3)–(6) can be expanded around the size parameter x_2. For example,

$$\begin{aligned}\psi_n(m_2x_1) &= \psi_n(m_2x_2 - m_2\epsilon)\\ &= \psi_n(m_2x_2) - (m_2\epsilon)\psi'_n(m_2x_2)\\ &\quad + (-m_2\epsilon)^2\psi''_n(m_2x_2)/2 + \ldots\end{aligned} \tag{33a}$$

and

$$\begin{aligned}\psi'_n(m_2x_1) &= \psi'_n(m_2x_2 - m_2\epsilon)\\ &= \psi'_n(m_2x_2) - (m_2\epsilon)\psi''_n(m_2x_2)\\ &\quad + (-m_2\epsilon)^2\psi'''_n(m_2x_2)/2 + \ldots,\end{aligned} \tag{33b}$$

where

$$\epsilon = x_2 - x_1 = 2\pi(r_2 - r_1)/\lambda. \tag{34}$$

Using the differential equation satisfied by the Ricatti–Bessel functions,

$$G''_n(z) + [1 - n(n+1)/z^2]G_n(z) = 0, \tag{35}$$

where $G_n(z) = \psi_n(z)$, $\chi_n(z)$, or $\zeta_n(z)$, Eqs. (33a) and (33b) can be recast in the following form:

$$\begin{aligned}\psi_n(m_2x_1) &= \psi_n(m_2x_2) - m_2\epsilon\psi'_n(m_2x_2)\\ &\quad + m_2^2\epsilon^2 t_n(m_2x_2)\psi_n(m_2x_2)/2 + \ldots,\end{aligned} \tag{36a}$$

$$\begin{aligned}\psi'_n(m_2x_1) &= \psi'_n(m_2x_2) - m_2\epsilon t_n(m_2x_2)\psi_n(m_2x_2)\\ &\quad + m_2^2\epsilon^2[t_n(m_2x_2)\psi_n(m_2x_2)]'/2 + \ldots,\end{aligned} \tag{36b}$$

where

$$t_n(m_2x_2) = n(n+1)/(m_2x_2)^2 - 1. \tag{37}$$

Thus the functions $\psi_n(m_2x_1)$ and $\psi'_n(m_2x_1)$ can each be expressed in a power series involving only the function $\psi_n(m_2x_2)$ and its single derivative $\psi'_n(m_2x_2)$. A similar analysis yields a power series in ϵ for each of the other functions $\chi_n(m_2x_1)$, $\chi'_n(m_2x_1)$, $\psi_n(m_1x_1)$, and $\psi'_n(m_1x_1)$ that occur in the analytical expressions for a_n and b_n [see Eqs. (1)–(6)]. In what follows, we assume that the shell is so thin that only the first-order term in ϵ need be retained in all the series expansions. With this assumption in mind, the numerator N_n [see Eqs. (1) and (3)] takes the form

$$N_n = \begin{vmatrix} \psi_n(x_2) & m_2\psi_n(m_2x_2) & m_2\chi_n(m_2x_2) & 0 \\ \psi'_n(x_2) & \psi'_n(m_2x_2) & \chi'_n(m_2x_2) & 0 \\ 0 & [m_2\psi_n(m_2x_2) & [m_2\chi_n(m_2x_2) & [m_1\psi_n(m_1x_2) \\ & -m_2^2\epsilon\psi'_n(m_2x_2)] & -m_2^2\epsilon\chi'_n(m_2x_2)] & -m_1^2\epsilon\psi'_n(m_1x_2)] \\ 0 & [\psi'_n(m_2x_2) - m_2\epsilon & [\chi'_n(m_2x_2) - m_2\epsilon & [\psi'_n(m_1x_2) - m_1\epsilon \\ & t_n(m_2x_2)\psi_n(m_2x_2)] & t_n(m_2x_2)\chi_n(m_2x_2)] & t_n(m_1x_2)\psi_n(m_1x_2)] \end{vmatrix} . \quad (38)$$

The above determinant can be written as the sum of four 4×4 determinants, one of which is independent of ϵ, two of which are linear in ϵ, and the remaining one is of order ϵ^2. Ignoring the last one, simplification of the others results in the following expression for N_n:

$$N_n = m_2 N_n^{(h)} - \epsilon(m_2^2 - m_1^2)R_n, \quad (39)$$

where

$$N_n^{(h)} = \psi'_n(m_1x_2)\psi_n(x_2) - m_1\psi_n(m_1x_2)\psi'_n(x_2), \quad (39a)$$

$$R_n = [n(n+1)/(m_2^2m_1x_2^2)]\psi_n(x_2)\psi_n(m_1x_2) + \psi'_n(x_2)\psi'_n(m_1x_2). \quad (39b)$$

Similarly,

$$D_n = m_2 D_n^{(h)} - \epsilon(m_2^2 - m_1^2)S_n, \quad (40)$$

where

$$D_n^{(h)} = \psi'_n(m_1x_2)\zeta_n(x_2) - m_1\psi_n(m_1x_2)\zeta'_n(x_2), \quad (40a)$$

$$S_n = [n(n+1)/(m_2^2m_1x_2^2)]\zeta_n(x_2)\psi_n(m_1x_2) + \zeta'_n(x_2)\psi'_n(m_1x_2). \quad (40b)$$

To first order in ϵ,

$$a_n = N_n/D_n = a_n^{(h)} + \epsilon\hat{a}_n, \quad (41)$$

where

$$a_n^{(h)} = N_n^{(h)}/D_n^{(h)} \quad (42)$$

and

$$\hat{a}_n = -i(m_2^2 - m_1^2)\{[\psi'_n(m_1x_2)]^2 + [n(n+1)/(m_2^2x_2^2)][\psi_n(m_1x_2)]^2\}/[D_n^{(h)}]^2. \quad (43)$$

In a similar fashion, the determinantal form of the scattering amplitude b_n [Eqs. (2), (5), and (6)] reduces to

$$b_n = b_n^{(h)} + \epsilon\hat{b}_n, \quad (44)$$

where

$$b_n^{(h)} = M_n^{(h)}/C_n^{(h)}, \quad (45)$$

$$M_n^{(h)} = m_1\psi'_n(m_1x_2)\psi_n(x_2) - \psi_n(m_1x_2)\psi'_n(x_2), \quad (46)$$

$$C_n^{(h)} = m_1\psi'_n(m_1x_2)\zeta_n(x_2) - \psi_n(m_1x_2)\zeta'_n(x_2), \quad (47)$$

and

$$\hat{b}_n = -i(m_2^2 - m_1^2)\{[\psi_n(m_1x_2)]^2\}/[C_n^{(h)}]^2. \quad (48)$$

$a_n^{(h)}$ and $b_n^{(h)}$ are the scattering amplitudes for a homogeneous sphere characterized by parameters m_1 and x_2. $\hat{a}_n$ and $\hat{b}_n$ represent the correction terms to first order in ϵ. It may be remarked here that these correction terms can also be obtained from a direct application of the set of boundary conditions valid for a thin spherical layer. These boundary conditions are derived in Appendix A.

The various cross sections are now given by

$$\sigma_{ext} = \sigma_{ext}^{(h)} + \epsilon\hat{\sigma}_{ext}, \quad (49)$$

$$\hat{\sigma}_{ext}^{(h)} = \frac{\lambda^2}{2\pi}\sum_n (2n+1)\mathrm{Re}[a_n^{(h)} + b_n^{(h)}], \quad (50a)$$

$$\sigma_{ext} = \frac{\lambda^2}{2\pi}\sum_n (2n+1)\mathrm{Re}(\hat{a}_n + \hat{b}_n), \quad (50b)$$

$$\sigma_{sca} = \sigma_{sca}^{(h)} + \epsilon\hat{\sigma}_{sca}, \quad (51)$$

where

$$\sigma_{sca}^{(h)} = \frac{\lambda^2}{2\pi}\sum_n (2n+1)[|a_n^{(h)}|^2 + |b_n^{(h)}|^2], \quad (52a)$$

$$\hat{\sigma}_{sca} = \frac{\lambda^2}{2\pi}\sum_n (2n+1)2\,\mathrm{Re}[\hat{a}_n a_n^{(h)*} + \hat{b}_n b_n^{(h)*}], \quad (52b)$$

$$\sigma_{abs} = \sigma_{ext} - \sigma_{sca} = [\sigma_{ext}^{(h)} - \sigma_{sca}^{(h)}] + \epsilon\frac{\lambda^2}{2\pi}\sum_n (2n+1) \times \mathrm{Re}\{\hat{a}_n[1 - 2a_n^{(h)*}] + \hat{b}_n[1 - 2b_n^{(h)*}]\}. \quad (53)$$

If m_1 is assumed to be real, Eq. (53) reduces to

$$\sigma_{abs} = -\epsilon\lambda^2 A/(2\pi), \quad (54)$$

where

$$A = \sum_n (2n+1)\mathrm{Im}[(m_2^2 - m_1^2)(\{[\psi'_n(m_1x_2)]^2 + [n(n+1)/(m_2^2x_2^2)][\psi_n(m_1x_2)]^2\}/|D_n^{(h)}|^2 + [\psi_n(m_1x_2)]^2/|C_n^{(h)}|^2)]. \quad (55)$$

Note that the factors $1/|D_n^{(h)}|^2$ and $|1/C_n^{(h)}|^2$ are the modulus squared of the internal field coefficients corresponding to the $a_n^{(h)}$ and the $b_n^{(h)}$ scattering amplitudes, respectively. They occur because the shell is embedded in a homogeneous spherical medium of refractive index m_1. When $m_1 = 1$, each one of them reduces to 1. Again, the quantity absorption cross section per unit volume (or mass) of the absorbing material can be evaluated. For σ_{abs} of Eq. (54), σ_{abs}/V is given by

$$\sigma_{abs}/V = \pi A/(\lambda x_2^2), \quad (56)$$

which is independent of ϵ, and a constant for a given set of parameters: m_1, m_2, and x_2. For the sake of illustration, we

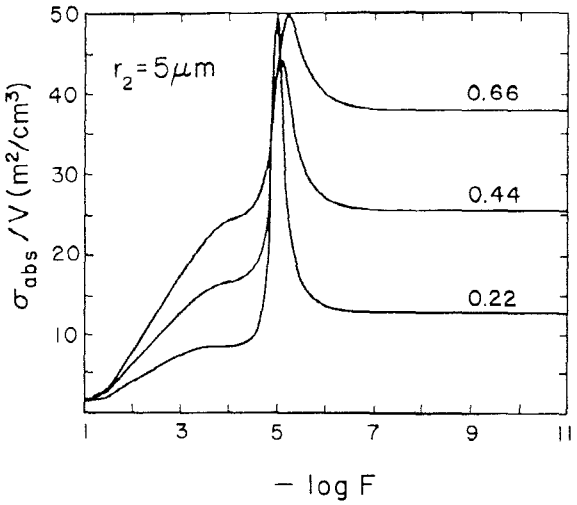

Fig. 8. Absorption cross section of water droplet ($m_1 = 1.33 - i0.0$) per unit volume of the shell ($m_2 = 2.0 - im_I$, $m_I > 0$) denoted by σ_{abs}/V as a function of its volume fraction F. The radius of the water droplet $r_2 = 5$ μm and the wavelength of light $\lambda = 0.5$ μm. Each curve is labeled by the value of m_I. $m_I = 0.66$ corresponds to graphitic carbon (soot).

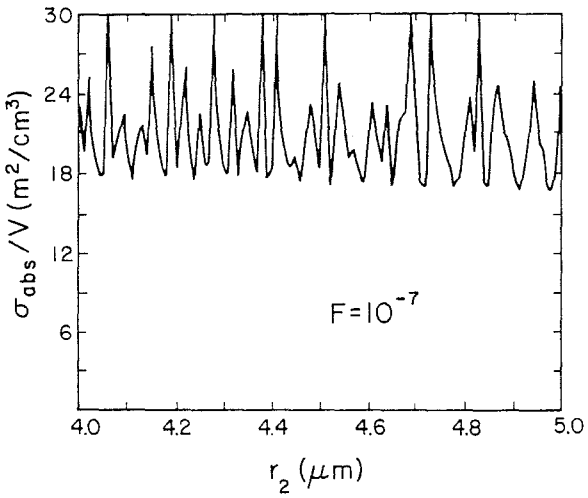

Fig. 9. Ripple structure in σ_{abs}/V for a soot-coated water droplet that is determined by the resonances in the internal field of a homogeneous water droplet of the same size. The volume fraction F of soot is 10^{-7}. The step size is 10^{-2} μm.

consider again the case of a water droplet ($m_1 = 1.33 - i0.0$) with graphitic carbon (soot) ($m_2 = 2.0 - i0.66$) this time forming a thin shell on the outside. We take $\lambda = 0.5$ μm and $r_2 = 5$ μm in the calculations. The calculations are performed by using the exact equations (see Section 2) and the numerical procedure given for the general case of a multilayered sphere in Ref. 7. The results are shown in Fig. 8. The top curve corresponds to the soot material. The other two curves are for different values of the imaginary part of the refractive index of the shell, as a further illustration. In each curve flatness is reached below $F = 10^{-6}$, as expected from Eq. (53). The limiting values in Fig. 8 again agree very well with those predicted by Eq. (56). In addition, they are seen to be proportional to the imaginary part of the refractive index m_2 in agreement with Eq. (55). The peaks[9] are due to a resonance explained below.

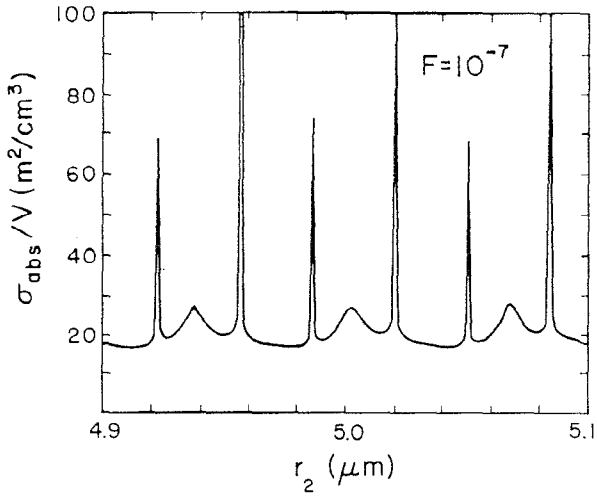

Fig. 10. Same as Fig. 9, except that the step size is 4×10^{-4} μm.

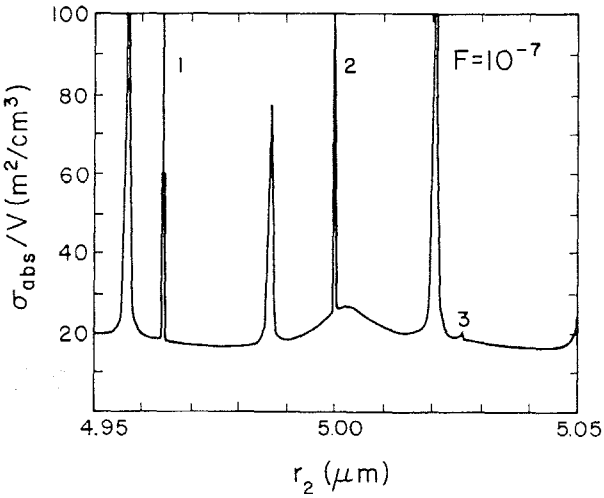

Fig. 11. Same as Fig. 10, except that a further reduction in step size to 2×10^{-4} μm reveals three more peaks labeled 1, 2, and 3. Peak 2 lies just beyond 5 μm.

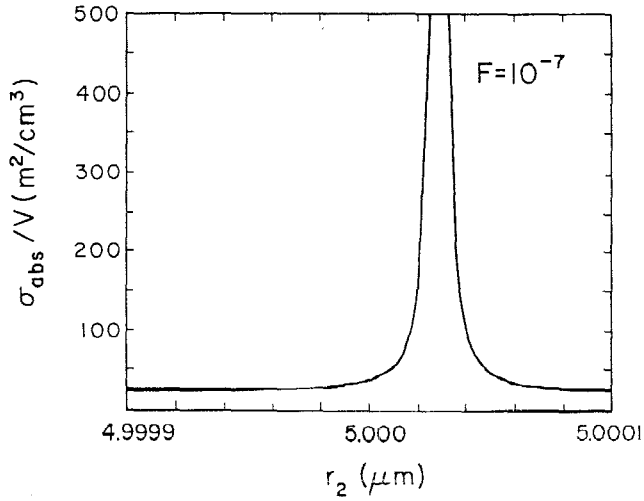

Fig. 12. Peak 2 of Fig. 11 shown in greater detail. It is due to a resonance in the electric mode, $n = 76$.

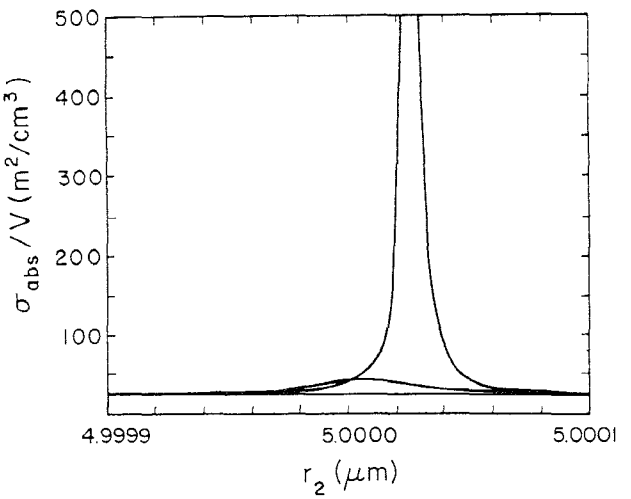

Fig. 13. Same as Fig. 12, except that F = 10^{-4} (flat curve), $F = 10^{-5}$ (the broad-peak curve), $F = 10^{-6}$ (the narrow-peak curve).

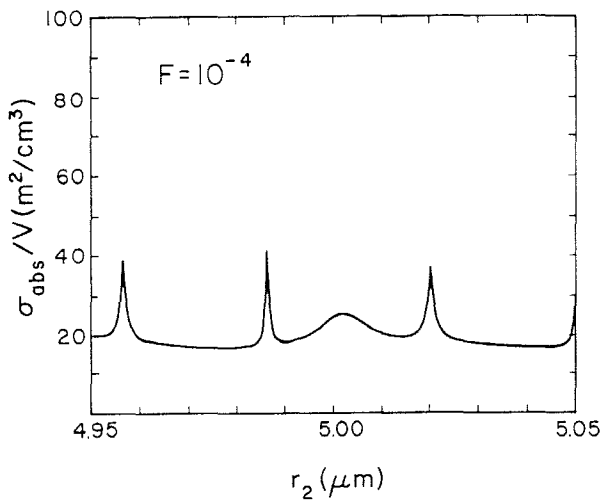

Fig. 14. Same as Fig. 11, except that $F = 10^{-4}$.

We next plot σ_{abs}/V as a function of the outer radius r_2 for a given volume fraction F. We take a low value such as $F = 10^{-7}$ so that Eq. (56) would remain essentially valid during the plot. Equation (54) shows that, as r_2 is varied, a pattern analogous to Mie scattering for a homogenous sphere (characterized by parameters m_2 and x_2) will emerge. In Fig. 9 we do see the ripple structure, which is to be expected considering the range of r_2. The radius r_2 is given increments of 0.01 μm in the plot. When the increment is reduced to 0.0004 μm, we obtain a plot shown in Fig. 10 for a narrow range of r_2 centered about 5 μm. More details are visible here than in the previous plot. However, the value of σ_{abs}/V for $r_2 = 5$ μm read from this plot does not agree with the value given by the plot in Fig. 8. The reason is that $r_2 = 5$ μm lies at the tail of a very narrow peak that is not revealed in Fig. 10. Further reduction of step size to 0.0002 μm uncovers this peak labeled 2 in Fig. 11. Peaks labeled 1 and 3, not visible earlier, also appear in this figure. Peak 2 is shown in greater detail in Fig. 12, where the step size is 10^{-6} μm. It has been identified as an enhancement in the electric mode of order $n = 76$. Exclusion of this partial-wave scattering amplitude results in the disappearance of this peak from Fig. 11.

In Fig. 12, we see that the peak rises beyond 500 m^2/cm^3. In fact, further calculations show that its value exceeds 22,000 m^2/cm^3. Narrow peaks such as those in Figs. 11 or 12 are a characteristic of very thin shells, which are due to the sharp resonant behavior of the internal field coefficients, expressed in Eq. (55) through the denominators $|D_n^{(h)}|^2$ and $|C_n^{(h)}|^2$. This feature is illustrated in Fig. 13, where the flat curve corresponds to a volume fraction F of 10^{-4} (or a thickness of $5 \times 10^{-4}/3$ μm). As F is reduced by a factor of 10 through 10^{-6}, which corresponds to a thickness of $5 \times 10^{-6}/3$ μm, which is less than the width of the peak, the narrow peak of Fig. 12 is resurrected. In Fig. 14 is given a plot of σ_{abs}/V for $F = 10^{-4}$ over a range of radius r_2 corresponding to the one in Fig. 11. Peaks labeled 1, 2, and 3 in Fig. 11 are no longer present in Fig. 14. The sharp but relatively broader peaks of Fig. 11 are present but with greatly diminished sizes. A further reduction of F to 10^{-3} also causes their disappearance. Thus the full spectrum of peaks revealed by Eq. (55) corresponding to first-order perturbation gradually diminishes as the shell thickness increases. Eventually, as the soot fills the entire volume, one obtains the plot corresponding to a homogeneous carbon particle in air (or in vacuum). Except for a broad peak (centered around $r = 0.08$ μm), σ_{abs}/V is a smoothly varying function of the radius of the particle in this plot.

5. CONCLUSION

Within a perturbative approach, we have provided analytic expressions for scattering by a single-layered sphere when either the core is tiny or the layer is thin. In the case of the tiny core, it is shown that the correction to Mie scattering owing to the presence of the core is a modified Rayleigh term determined by an incident wave that is the internal field corresponding to a homogeneous sphere. When the shell is nonabsorbing and the core absorbing, the absorption cross section for the composite particle is calculated and applied to the case of absorption of visible light ($\lambda = 0.5$ μm) by a water droplet containing a tiny graphitic-carbon (soot) core. Results for the absorption cross section per unit volume of soot versus the radius of the water droplet predict oscillations, which are identified with resonances in the internal field of the nonabsorbing water droplet, corresponding to the electric-dipole mode ($n = 1$). On the other hand, in the case of the thin shell, the internal coefficients corresponding to all the modes of oscillation determine the correction term. When applied to the case of a water droplet with a soot shell, narrow peaks analogous to the ripple structure[10] in Mie scattering become visible in the absorption cross section per unit volume as a function of the radius r_2. These peaks are due to resonances in the internal field of the nonabsorbing water droplet. This ripple structure is not to be confused with the ripple structure in the absorption cross section of a weakly absorbing homogeneous sphere.[11] As the shell thickness increases, the observed ripple structure dies gradually. In other words, the perturbation procedure revealing the peaks is no longer valid.

Finally, we remark that it would be interesting to make an experimental observation of the aforementioned narrow peaks, as it would be an explicit proof of the narrow internal resonance predicted by Mie theory. In the water–soot example considered in this paper, these peaks appear for vol-

ume fractions $\leq 10^{-4}$ for a water droplet of radius $r_2 = 5\ \mu$m, too low to correspond to a physically possible thickness of the soot layer. However, if we note that the equations depend on the size parameter x_2 ($= 2\pi r_2/\lambda$), an experimental verification of the narrow peaks can be made possible in a laboratory with the use of longer wavelengths (e.g., microwaves), provided that a different pair of materials, one absorbing (for the shell) and the other nonabsorbing or weakly absorbing (for the core), exists. The requirement that $x_2 \gg 1$ to unravel the peaks is easily satisified in this case by scaling the radii of the single-layered sphere accordingly. As a consequence of these large radii, physically meaningful thicknesses for the layer are then possible for low volume fractions of the absorbing material.

APPENDIX A: BOUNDARY CONDITIONS AT A THIN SPHERICAL LAYER

Approximate boundary conditions at a thin spherical layer immersed in a vacuum were given by Andreasen[12,13] several years ago, in connection with the study of scattering properties of a dielectric bubble. Scattering amplitudes (also approximate) were subsequently derived from these boundary conditions. In this appendix, we derive the boundary conditions in their complete form and in a very general way. These boundary conditions are found to lead to precisely the same form of analytic expressions for scattering amplitudes for a single-layered sphere with a thin shell as those given in Section 4 of this paper.

Figure 15 shows a tiny portion of a spherical shell of refractive index m_2 separating the core of radius r_1 and refractive index m_1 from the external medium of refractive index m_3. The tangential components of the fields at the two interfaces (in particular, at points a and b in Fig. 15) satisfy the following boundary conditions:

$$\hat{n} \times [\mathbf{E}_3(\mathbf{r}_2) - \mathbf{E}_2(\mathbf{r}_2)] = 0, \tag{A1a}$$

$$\hat{n} \times [\mathbf{E}_2(\mathbf{r}_1) - \mathbf{E}_1(\mathbf{r}_1)] = 0, \tag{A1b}$$

$$\hat{n} \times [\mathbf{H}_3(\mathbf{r}_2) - \mathbf{H}_2(\mathbf{r}_2)] = 0, \tag{A2a}$$

$$\hat{n} \times [\mathbf{H}_2(\mathbf{r}_1) - \mathbf{H}_1(\mathbf{r}_1)] = 0, \tag{A2b}$$

where $\mathbf{E}_i$ and similarly $\mathbf{H}_i$ refer to the field inside medium i. $\hat{n}$ is the unit vector defining the common directions of vectors $\mathbf{r}_1$ and $\mathbf{r}_2$ that correspond to some angle θ, ϕ in a three-dimensional coordinate system. $\hat{\theta}$ and $\hat{\phi}$ are the other unit vectors tangential to the spherical surface. In what follows, we assume that $\Delta r = r_2 - r_1$ is very small.

We consider the set of Eqs. (A2a) and (A2b) first and observe that $\mathbf{H}_2(\mathbf{r}_1)$ can be written to first order in Δr as

$$\mathbf{H}_2(\mathbf{r}_1) = \mathbf{H}_2(\mathbf{r}_2) - \Delta\mathbf{r} \cdot \nabla\mathbf{H}_2(\mathbf{r}_2). \tag{A3a}$$

In a similar way, we can write

$$\mathbf{H}_1(\mathbf{r}_1) = \mathbf{H}_1(\mathbf{r}_2) - \Delta\mathbf{r} \cdot \nabla\mathbf{H}_1(\mathbf{r}_2), \tag{A3b}$$

where $\mathbf{H}_1(\mathbf{r}_2)$ is the extrapolation of $\mathbf{H}_1(\mathbf{r}_1)$ to $\mathbf{r} = \mathbf{r}_2$. These results in conjunction with Eqs. (A2a) and (A2b) then give

$$\hat{n} \times [\mathbf{H}_3(\mathbf{r}_2) - \mathbf{H}_1(\mathbf{r}_2)] = \Delta r \hat{n} \times [(\hat{n} \cdot \nabla)(\mathbf{H}_2 - \mathbf{H}_1)]_{\mathbf{r}=\mathbf{r}_2}. \tag{A4}$$

Use of the vector identity

$$\nabla(\mathbf{A} \cdot \mathbf{B}) = (\mathbf{B} \cdot \nabla)\mathbf{A} + (\mathbf{A} \cdot \nabla)\mathbf{B} + \mathbf{B} \times (\nabla \times \mathbf{A}) + \mathbf{A} \times (\nabla \times \mathbf{B}) \tag{A5}$$

and the Maxwell equation

$$\nabla \times \mathbf{H} = i(\omega/c)\epsilon\mathbf{E} \tag{A6}$$

further renders Eq. (A4) into the following form:

$$\hat{n} \times [\mathbf{H}_3(\mathbf{r}_2) - \mathbf{H}_1(\mathbf{r}_2)] = \Delta r(i\omega/c)\{\hat{n} \times [\epsilon_2\mathbf{E}_2(\mathbf{r}_2) - \epsilon_1\mathbf{E}_1(\mathbf{r}_2)]\} \times \hat{n} + \Delta r \hat{n} \times \nabla[(\mathbf{H}_2 - \mathbf{H}_1) \cdot \hat{n}]_{\mathbf{r}=\mathbf{r}_2} - (\Delta r/r_2)\, \hat{n} \times [\mathbf{H}_3(\mathbf{r}_2) - \mathbf{H}_1(\mathbf{r}_2)]. \tag{A7}$$

Note that Eq. (A6) assumes a time dependence of the form $\exp(i\omega t)$ for the fields. Also, ϵ_j denotes the dielectric constant of medium j. The second term in Eq. (A7) involves the difference in the tangential components of the gradient of H_r (the radial component of $\mathbf{H}$) evaluated at $\mathbf{r} = \mathbf{r}_2$. Using Eq. (A1a) and the continuity of the radial component of $\mu\mathbf{H}$ at the interface $\mathbf{r} = \mathbf{r}_2$ (μ denotes permeability), Eq. (A7) to first order in Δr can then be reexpressed as follows:

$$\hat{n} \times [\mathbf{H}_3(\mathbf{r}_2) - \mathbf{H}_1(\mathbf{r}_2)] = \Delta r(i\omega/c)\{\hat{n} \times [\epsilon_2\mathbf{E}_3(\mathbf{r}_2) - \epsilon_1\mathbf{E}_1(\mathbf{r}_2)]\} + \Delta r\mu_3(1/\mu_2 - 1/\mu_1)\hat{n} \times \nabla(\mathbf{H}_3 \cdot \hat{n})_{\mathbf{r}=\mathbf{r}_2}. \tag{A8}$$

A similar analysis, beginning with Eqs. (A1a) and (A1b), yields

$$\hat{n} \times [\mathbf{E}_3(\mathbf{r}_2) - \mathbf{E}_1(\mathbf{r}_2)] = \Delta r(-i\omega/c) \times \{\hat{n} \times [\mu_2\mathbf{H}_3(\mathbf{r}_2) - \mu_1\mathbf{H}_1(\mathbf{r}_2)]\} \times \hat{n} + \Delta r\epsilon_3(1/\epsilon_2 - 1/\epsilon_1)\hat{n} \times \nabla(\mathbf{E}_3 \cdot \hat{n})_{\mathbf{r}=\mathbf{r}_2}. \tag{A9}$$

Equations (A8) and (A9) constitute a pair of boundary conditions applied at the outer surface of a thin shell of refractive index m_2 separating two media, the outer one of refractive index m_3 and the inner of refractive index m_1. $m_i = \sqrt{\epsilon_i\mu_i}$, $i = 1, 2, 3$. This is to be contrasted with the set of four conditions, Eqs. (A1a) and (A1b) and Eqs. (A2a) and (A2b), that normally need to be satisfied in the general case of a

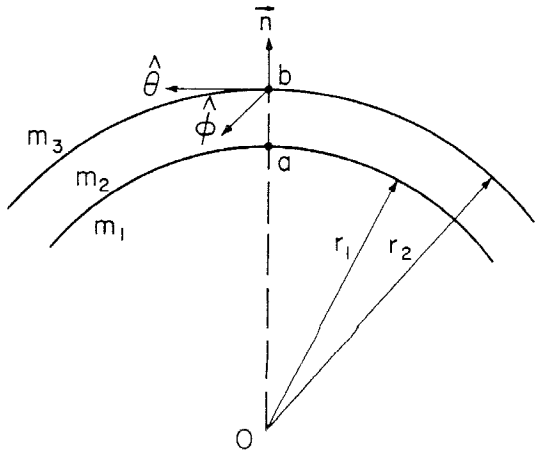

Fig. 15. Geometry of a spherical shell of refractive index m_2. The refractive indices of the core and the external medium are m_1 and m_3, respectively.

spherical layer. As expected, the right-hand sides of Eqs. (A8) and (A9) reduce to zero when $\mu_2 = \mu_1$ and $\epsilon_2 = \epsilon_1$. In the case of $\mu_2 = \mu_1$, Eqs. (A8) and (A9) reduce to

$$\hat{n} \times [\mathbf{H}_3(\mathbf{r}_2) - \mathbf{H}_1(\mathbf{r}_2)] = \Delta r(i\omega/c) \times \{\hat{n} \times [\epsilon_2 \mathbf{E}_3(\mathbf{r}_2) - \epsilon_1 \mathbf{E}_1(\mathbf{r}_2)]\} \times \hat{n}, \tag{A10}$$

$$\hat{n} \times [\mathbf{E}_3(\mathbf{r}_2) - \mathbf{E}_1(\mathbf{r}_2)] = \Delta r \epsilon_3 (1/\epsilon_2 - 1/\epsilon_1) \times \hat{n} \times \nabla(\mathbf{E}_3 \cdot \hat{n})_{\mathbf{r}=\mathbf{r}_2}. \tag{A11}$$

The first term on the right-hand side of Eq. (A9) becomes of order $(\Delta r)^2$ by virtue of Eq. (A10) and is therefore dropped in Eq. (A11). When Eqs. (A10) and (A11) are applied to scattering in vacuum ($m_3 = 1$) by a single-layered sphere with a thin shell with $\mu_1 = \mu_2 = 1$, one obtains precisely the same analytic expressions for scattering amplitudes as those obtained earlier in Section 4 of this paper. It is the right-hand side of Eq. (A11) that is responsible for the term containing the factor $n(n+1)/(m_2^2 x_2^2)$ in the analytic expression for $\hat{a}_n$ in Eq. (43). $x_2 = 2\pi r_2/\lambda$. If m_2 is very large, this term can be ignored. In Eq. (A11), it corresponds to setting the right-hand side to zero. This result in conjunction with Eq. (A10) then implies that

$$\hat{n} \times [\mathbf{H}_3(\mathbf{r}_2) - \mathbf{H}_1(\mathbf{r}_2)] = (\Delta r)(i\omega/c)(\epsilon_2 - \epsilon_1)\,(\hat{n} \times \mathbf{E}_3) \times \hat{n}. \tag{A12}$$

This approximate boundary condition with $\epsilon_1 = 1$ acquires the same form as the one given by Andreasen[13] for a dielectric bubble in vacuum.

In short, we have given the precise form of the boundary conditions at a thin spherical layer [Eqs. (A10) and (A11)]. This derivation is based on a formal treatment and is exact up to first order in shell thickness. Although we have discussed the results of its application to a single-layered case, it can be applied to a thin layer within a multilayered sphere. For example, the partial-wave scattering amplitudes for a thin carbon shell embedded within a water droplet, to first order in the shell thickness, may be obtained by the direct application of Eqs. (A10) and (A11). Equation (A12) is an approximate form of the type given earlier by Andreasen[13] using a less formal approach. For $m_1 = 1.33 - i0.0$, $m_2 = 1.0 - i0.66$, $m_3 = 1.0$, $\lambda = 0.5\ \mu$m, r_2 varying from 0.01 to 10 μm, and a fixed volume fraction of 10^{-6} for the layer, calculations for the absorption cross section based on Eq. (A12) give errors from 20 to 40%. If, however, m_2 is changed to $5.0 - i0.66$, the error is of the order of 0.1%.

REFERENCES AND NOTES

1. R. W. Fenn and H. Oser, "Scattering properties of concentric soot–water spheres for visible and infrared light," Appl. Opt. **4,** 1504–1509 (1965).
2. R. E. Danielson, D. R. Moore, and H. C. van de Hulst, "The transfer of visible radiation through clouds," J. Atmos. Sci. **26,** 1078–1087 (1969).
3. H. Rosen, D. A. Hansen, R. L. Dod, and T. Novakov, "Soot in urban atmospheres: determination by an optical absorption technique," Science **208,** 741–744 (1980).
4. T. P. Ackerman and O. B. Toon, "Absorption of visible radiation in atmosphere containing mixtures of absorbing and nonabsorbing particles," Appl. Opt. **20,** 3661–3668 (1981).
5. P. Chylek, V. Ramaswamy, and R. J. Cheng, "Effect of graphitic carbon on the albedo of clouds," J. Atmos. Sci. **41,** 3076–3084 (1984).
6. M. Kerker, *The Scattering of Light and Other Electromagnetic Radiation* (Academic, New York, 1969).
7. R. Bhandari, "Scattering coefficients for a multilayered sphere: analytic expressions and algorithms," Appl. Opt. **24,** 1960–1967 (1985).
8. See, for example, D. M. Roessler, D. S. Y. Wang, and M. Kerker, "Optical absorption by randomly oriented carbon spheroids," Appl. Opt. **22,** 3648–3651 (1983), and Ref. 5.
9. We point out here that a peak similar to the one corresponding to $m_2 = 2.0 - i0.66$ in Fig. 8 should be present in Fig. 4 of Ref. 5, even though the refractive indices used there for carbon ($1.94 - i0.66$) and water ($1.33 - i10^{-9}$) are slightly different. Our calculations bear this out.
10. H. C. van de Hulst, *Light Scattering by Small Particles* (Wiley, New York 1957); P. Chylek, J. T. Kiehl, and M. K. W. Ko, "Narrow resonance structure in the Mie scattering characteristics," Appl. Opt. **17,** 3019–3021 (1978).
11. H. S. Bennett and G. J. Rosasco, "Resonances in the efficiency factors for absorption: Mie scattering theory," Appl. Opt. **17,** 491–493 (1978).
12. M. G. Andreasen, "Back-scattering cross section of a thin, dielectric spherical shell," IRE Trans. Antennas Propag. **AP-5,** 267–270 (1957).
13. M. G. Andreasen, "Radiation from a radial dipole through a thin dielectric spherical shell," IRE Trans. Antennas Propag. **AP-5,** 337–342 (1957).